NRC Research Press

ARTICLE

An improved canopy wind model for predicting wind adjustment factors and wildland fire behavior

W.J. Massman, J.M. Forthofer, and M.A. Finney

Abstract: The ability to rapidly estimate wind speed beneath a forest canopy or near the ground surface in any vegetation is critical to practical wildland fire behavior models. The common metric of this wind speed is the "mid-flame" wind speed, U^{MF}. However, the existing approach for estimating U^{MF} has some significant shortcomings. These include the assumptions that both the within-canopy wind speed and the canopy structure are uniform with depth (z) throughout the canopy and that the canopy roughness length (z_0) and displacement height (d) are the same regardless of canopy structure and foliage density. The purpose of this study is to develop and assess a model of canopy wind and Reynolds stress that eliminates these shortcomings and thereby provide a more physically realistic method for calculating U^{MF}. The present model can be used for canopies of arbitrary plant surface distribution and leaf area, and the single function that describes the within-canopy wind speed is shown to reproduce observed canopy wind speed profiles across a wide variety of canopies. An equally simple analytical expression for the within-canopy Reynolds stress, $u_*^2(z)$, also provides a reasonable description of the observed vertical profiles of Reynolds stress. In turn, $u_*^2(z)$ is used to calculate z_0 and d. Tests of operational performance are also discussed.

Key words: fire spread modeling, canopy foliage distribution, Rothermel model.

Résumé : La capacité d'estimer rapidement la vitesse du vent sous un couvert forestier ou près de la surface du sol peu importe la formation végétale est essentielle pour les modèles pratiques de comportement des feux de forêt. La métrique commune de cette vitesse du vent est la vitesse du vent à « mi-flamme », U^{MF}, mais la façon courante d'estimer U^{MF} comporte d'importantes lacunes. Celles-ci incluent les hypothèses qu'à la fois la vitesse du vent dans le couvert forestier et la structure du couvert forestier sont uniformes peu importe la profondeur (z) partout dans le couvert et que la longueur de rugosité du couvert (z_0) et le plan de vitesse nulle (d) sont identiques peu importe la structure du couvert et la densité du feuillage. Le but de cette étude consiste à élaborer et évaluer un modèle de vent dans le couvert et de tension de Reynolds qui élimine ces lacunes et fournit ainsi une méthode physiquement plus réaliste pour calculer U^{MF}. Ce modèle peut être utilisé pour les couverts où la répartition de la surface végétale et la surface foliaire sont arbitraires et la fonction unique qui décrit la vitesse du vent à l'intérieur du couvert reproduit les profils de vitesse du vent observés pour une grande variété de couverts forestiers. Une expression analytique également simple de la tension de Reynolds à l'intérieur du couvert, $u_*^2(z)$, fournit elle aussi une description raisonnable des profils verticaux de tension de Reynolds selon les valeurs observées. À son tour, $u_*^2(z)$ est utilisé pour calculer z_0 et d. Des tests de performance opérationnelle font aussi l'objet de la discussion. [Traduit par la Rédaction]

Mots-clés : modélisation de la propagation du feu, répartition du feuillage dans le couvert forestier, modèle de Rothermel.

Introduction

Wildland fire behavior is strongly influenced by the ambient wind that impinges on the flame zone. For most fires, this "mid-flame" wind (Rothermel 1972) is closer to the ground than winds measured at a standard reference height above the vegetation (10 m international or 20 feet US). A method is required to obtain mid-flame winds, which are reduced by a forest canopy and vegetation roughness, from observations or forecasts of winds at the reference height. This reduction factor, often referred to as the "wind adjustment factor" (WAF < 1 (dimensionless)), was first modeled by Albini and Baughman (1979) (AB79). For practical modeling purposes, a method of estimating mid-flame wind using the WAF must satisfy two criteria: it must be numerically efficient and it must be robust to the uncertainties inherent in knowing vegetation structure at an arbitrary place on a vast landscape. The model of AB79 meets these objectives and is consequently widely used in

US fire behavior prediction systems (Andrews 2012). However, to achieve this ease of use and utility, the AB79 model required some significant compromises to physical realism. In particular, AB79 assume that the within-canopy wind profile, $u(z)$ (m·s⁻¹), is uniform throughout the canopy. Furthermore, it does not allow for the possibility (e.g., Shaw and Pereira 1982) that plant surface area density distribution, ($a(z)$, m²·m⁻³; also known as the plant area density or PAD), foliage amount (m²·m⁻²; plant area index or PAI), and foliage drag coefficient ($C_d(z)$, dimensionless) can influence or modulate $u(z)$. And finally, the logarithmic wind speed profile above the canopy, which is central to AB79, requires knowledge of the canopy roughness length (z_0, m) and displacement height (d, m). But AB79 assume fixed values for the ratios of z_0 and d to canopy height (i.e., $z_0/h \approx 1/8$ and $d/h \approx 2/3$, where h (m) is canopy height) that are most appropriate to full canopy cover. Consequently, the AB79 WAF model does not allow for the possible influence of canopy structure and foliage density on z_0/h and d/h (e.g., Shaw and

Pereira 1982; Massman 1987). This could be a disadvantage when calculating WAF for fires that occur within grasslands and shrublands, because these ecosystems are often more appropriately considered partial canopy cover, rather than full canopy cover, and they both have very different plant surface distribution and drag characteristics from one another and from full forested canopies.

Wildland fire behavior can also be strongly influenced by any fire-induced winds, which are not explicit or appropriate to either AB79 or the present study because such winds are (at least partially) implicit within the Rothermel Fire Spread Model (RFSM; Rothermel 1972). There are historical reasons for this, which are associated with the original development of the RFSM. The RFSM was developed by correlating fire spread rates of a linear flame zone with the constant, uniform, and steady wind speeds generated within a wind tunnel before the fire was ignited. Therefore, at least for these wind tunnel experiments, any fire-induced wind effects are implicitly included with the observed spread rates. By intention, therefore, RFSM is an extremely simple analog to what is in reality an extraordinarily complex and dynamic physical phenomenon, which is well beyond the intention of either the present study or AB79. However, this does not mean that AB79 cannot be improved upon.

This paper describes a model and an approach that seeks to improve upon the physical realism of the AB79 model without sacrificing model utility. Specifically, the present model introduces a new method for estimating the canopy WAF for use with the RFSM. (Note: the RFSM could more appropriately be termed the Rothermel Fire Spread Equation, but we prefer to use 'Model'). This model is based on analytical expressions (developed and evaluated in the following sections) for both the canopy wind speed and Reynolds stress, $u_*^2(z)$ (m²·s⁻²), that can be used for vegetation canopies of any arbitrary plant surface distribution, density, and drag characteristics. The model is then extended to give estimates of z_0/h and d/h that are consistent with the assumed $a(z)$, PAI, and $C_d(z)$ using (i) Thom's (1971) suggestion that the displacement height corresponds to the effective level of mean drag upon the canopy elements, and (ii) a simple analytical expression for the bulk drag coefficient of the vegetated surface, C_{surf} (dimensionless; e.g., Massman 1997), where C_{surf} refers to the combined effects of all the canopy elements and the soil surface. Once $u(z)$, d/h, and z_0/h have been determined, it is a fairly simple matter to determine the values of the corresponding canopy and surface WAFs. Finally, we compare fire behavior output from the RFSM using WAFs from both the present wind model and AB79.

A general canopy wind and stress model

In the broadest terms, the model being proposed here belongs to a general class of one-dimensional analytical models originally developed over 50 years ago (Inoue 1963; Cionco 1965; Cowan 1968). Since that time, these models have been extended and generalized for a variety of purposes (e.g., Albini 1981; Massman 1987, 1997; Raupach et al. 1996; Yi 2008; Queck and Bernhofer 2010; Wang 2012; de Souza et al. 2016). Critiques of some of these later models have suggested that they may lack a sound theoretical basis (Finnigan et al. 2015). This may be one reason that variants on Inoue's original 1963 exponential within-canopy wind model are often basic to larger scale plant–atmosphere models (e.g., Su et al. 2001; Harman and Finnigan 2007). Nonetheless, even these more frequently employed analytical models fail to satisfy the expected no-slip lower boundary condition. The model developed here satisfies that lower boundary condition while retaining a fairly simple analytical expression. Consequently, this new model should find application well beyond the fire-related modeling outlined in this study.

The present model is a combination or adaptation of the one-dimensional (vertically varying) canopy wind models of Massman (1987) (M87) and Massman (1997) (M97). Both of these models assume and (or) derive simple analytical expressions for the within-

canopy horizontal wind and stress profiles and are useful to the present study because of their simplicity and ease of computation and because they both allow for variable (or non-uniform) plant surface distribution. The M87 model is based on a triangular plant surface distribution and M97's model can be used with any completely arbitrary plant surface distribution. Although both models give reasonable descriptions of the wind and stress profiles within full canopies (i.e., those canopies characterized by a PAI > ~1), they are not necessarily as useful for thinner canopies or canopies that only partially cover the surface. In general terms, these analytical models tend to fail as the canopy becomes progressively thinner (i.e., as PAI → 0), because the lower boundary condition on the canopy wind and stress profiles in both models is most suitable for the full canopy cover (PAI ≥ 1) and becomes progressively less suitable as PAI decreases. The present model resolves this dilemma by establishing a (mathematically continuous) within-canopy wind profile that fulfills a no-slip lower boundary condition (i.e., the wind speed at the bottom of the canopy is approximately logarithmic in shape and the wind speed diminishes to zero at the roughness length of the ground surface) regardless of canopy density (PAI) or canopy structure ($a(z)$).

The next two sections present the explicit mathematical expressions that describe the plant surface distribution and related model variables and the models for the wind and stress profiles. Both sections also include comparisons between the models and observations.

Note that for the remainder of this manuscript, many of the physical variables and parameters are expressed nondimensionally in terms of the canopy height. For example, vertical height above the ground, z, is expressed $\xi = z/h$ and the plant surface distribution, $a(z)$, is expressed as $ha(\xi)$. This nondimensionalization allows the internal computations of the model to remain independent of a specific canopy height, which is input separately and externally when actually performing the WAF calculations.

Foliage area and drag area distributions and drag area index

Following M97, the nondimensional plant surface distribution function, $ha(z)$, is constructed as follows:

$$(1) \qquad ha(\xi) = \text{PAI} \frac{f_a(\xi)}{\int_0^1 f_a(\xi')d\xi'}$$

where $f_a(\xi)$ (dimensionless) is an arbitrary function for $0 \leq \xi \leq 1$ (i.e., $0 \leq z \leq h$) that describes the desired mathematical shape of the plant surface distribution, e.g., a triangular shape (Shaw and Pereira 1982), a modified β distribution shape or a normal distribution shape (Massman 1982), or a piecewise continuous function that describes the measured canopy structure (Halldin 1985); and ξ' is a variable of integration signifying the integration of f_a over the depth of the canopy. This integration normalizes $f_a(\xi)$ and ensures that PAI $= \int_0^1 ha(\xi')d\xi'$ as required.

Figures 1 and 2 are a series of plots of the observed and modeled $f_a(\xi)$ for the eight different canopies discussed by Katul et al. (2004) and M87. The modeled $f_a(\xi)$ shown in these figures is termed an "asymmetric Gaussian" because the standard deviation (σ_u, dimensionless) above the height of maximum foliage area density, $\xi_{max} \leq 1$, can be different from that below ξ_{max}, for which the standard deviation is σ_l, or more explicitly

$$(2) \qquad f_a(\xi) = \begin{cases} \exp\left(\dfrac{-(\xi - \xi_{max})^2}{\sigma_u^2}\right) & \xi_{max} \leq \xi \leq 1 \\ \exp\left(\dfrac{-(\xi_{max} - \xi)^2}{\sigma_l^2}\right) & 0 \leq \xi \leq \xi_{max} \end{cases}$$

Fig. 1. Foliage distribution shape functions, $f_a(z/h)$, for aspen, Scots pine, jack pine, and loblolly pine canopies. Shaded areas are observationally based and the fit with the asymmetric Gaussian model (eq. 2) along with its associated parameter values (ξ_{max}, σ_u, σ_l, respectively) are given in blue. [Colour online.]
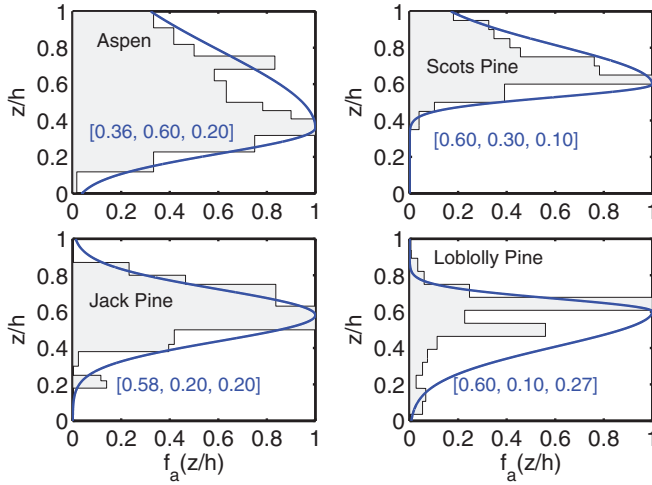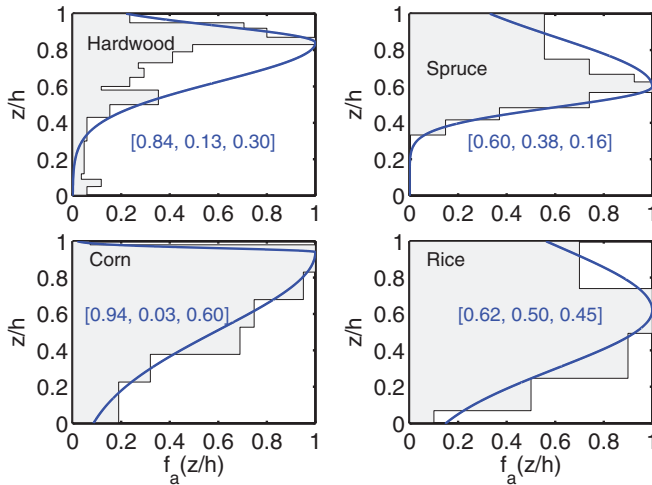

Fig. 2. Foliage distribution shape functions, $f_a(z/h)$, for a hardwood forest, spruce, corn, and rice canopies. Shaded areas are observationally based and the fit with the asymmetric Gaussian model (eq. 2) along with its associated parameter values (ξ_{max}, σ_u, σ_l, respectively) are given in blue. [Colour online.]

For most of the present study, this asymmetric Gaussian is used in place of the observed $f_a(\xi)$ because it does provide smoother canopy wind and stress profiles, as well as a smoother $f_a(\xi)$, without compromising the model's performance in any way. It is also worthy of note that none of the six forest canopies shown in these two figures display much of an understory, i.e., they do not exhibit a secondary increase in $a(z)$ within the lower 20% or so of the canopy. This lack of an understory benefits the present study, because it allows the parameterization of $a(z)$ to be relatively simple (requiring only three parameters). However, there are no inherent barriers within the model that prevent including an understory because the shape function $f_a(\xi)$ is completely arbitrary. In fact, a few test runs were made with a fictitious understory added to $a(z)$. As long as the understory C_dPAI is small compared with the overstory C_dPAI, which is usually the case, its influence on the modeling results were mostly negligible.

Again following M97, the drag area distribution is the product of the leaf area distribution and the bulk drag coefficient, $c_d(\xi)$,

associated with the ensemble of all foliage elements at any given height.

$$(3) \qquad c_d(\xi) = C_d\left[\frac{e^{-d_1(1-\xi)}}{1 + p_1ha(\xi)}\right]$$

where C_d (dimensionless) is the drag coefficient of the individual foliage elements; $[1+p_1ha(\xi)]$ with $p_1 \geq 0$ is the shelter factor, which when $p_1 > 0$ allows for the reduction of the foliage drag forces whenever the canopy elements shelter (or block) one another from direct exposure to the wind; and the term $\exp(-d_1(1-\xi))$ with $|d_1| \geq 0$ allows for the drag coefficient to vary with height independent of any sheltering. This last term is intended to emulate the condition that $c_d(\xi)$ may be directly ($d_1 > 0$) or inversely ($d_1 < 0$) proportional to wind speed (Grant 1983, 1984) or possibly proportional to some non-integer power of the wind speed. M97 discusses these two parameterizations in greater detail, and for the present purposes, the default values for d_1 and p_1 are zero. However, as discussed in the following section, it was found that for two canopies, the new canopy wind model's performance was enhanced by adjusting d_1.

Just as PAI is the integral of the plant surface distribution over the depth of the canopy, the drag area index, $\zeta(h)$, is the integral of the drag area distribution over the depth of the canopy

$$(4) \qquad \zeta(h) \equiv \int_0^1 c_d(\xi')ha(\xi')d\xi'$$

which, in the default case of $p_1 \equiv 0$ and $d_1 \equiv 0$, means that $\zeta(h) \equiv C_d$PAI.

Finally, and similar to M97, the present wind model is also developed in terms of the cumulative drag area, $\zeta = \zeta(\xi)$, which is defined as follows:

$$(5) \qquad \zeta(\xi) = \int_0^\xi c_d(\xi')ha(\xi')d\xi'$$

This model variable replaces the height variable, ξ, in the mathematical formulation for wind speed so that $u = u(\zeta(\xi))$, which will be shortened to $u = u(\xi)$. Also note that we have specifically chosen to use the symbol $\zeta(h)$ in place of $\zeta(1)$ in eq. 4 to emphasize the importance of drag area index to the model and to maintain the same notation as M97. The within-canopy wind speed, u, is defined next.

Canopy wind and stress profiles

The nondimensional canopy wind speed profile, $u(z)/u(h) \equiv u(\xi)/u(1)$, is the product of two terms: the first, $U_b(\xi)$, is logarithmic and dominant near the ground and the lower part of the canopy and the second, $U_t(\xi)$, is a hyperbolic cosine and dominates near the top of the canopy.

$$(6) \qquad U_b(\xi) = \begin{cases} \dfrac{\log(z/z_{0G})}{\log(h/z_{0G})} = \dfrac{\log(\xi/\xi_{0G})}{\log(1/\xi_{0G})} & z_{0G} \leq z \leq h \\ 0 & 0 \leq z \leq z_{0G} \end{cases}$$

and

$$(7) \qquad U_t(\xi) = \frac{\cosh[N\zeta(\xi)/\zeta(h)]}{\cosh(N)} \qquad 0 \leq z \leq h$$

where z_{0G} (m) is the roughness length of the ground surface and $\xi_{0G} \equiv z_{0G}/h = 0.0025$ by default assignment for the present and N is taken directly from M97:

Fig. 3. Blue (canopy wind speed profiles): comparison of observed data (symbols) and model results (lines, eq. 11). Red (canopy stress profiles): comparison of observed data (symbols), analytical model results (solid lines, eq. 12), and numerically integrated results (dashed lines, eq. 13). These canopies correspond to those in Fig. 1.

Fig. 4. Blue (canopy wind speed profiles): comparison of observed data (symbols) and model results (lines, eq. 11). Red (canopy stress profiles): comparison of observed data (symbols), analytical model results (solid lines, eq. 12), and numerically integrated results (dashed lines, eq. 13). These canopies correspond to those in Fig. 2.
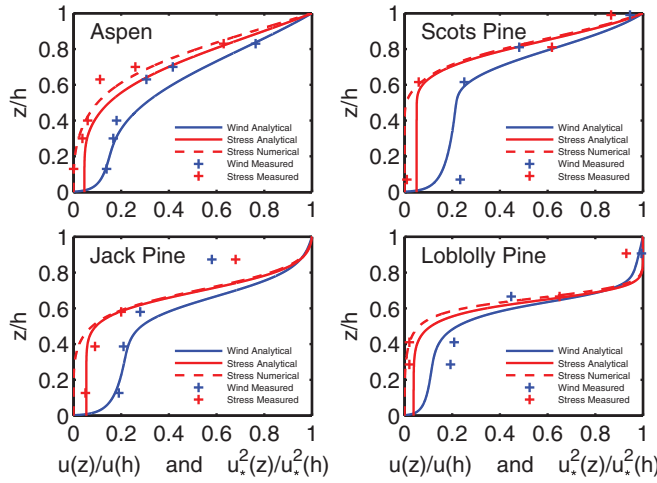
$$(8) \qquad N = \frac{\zeta(h)}{C_{surf}}$$

with

$$(9) \qquad C_{surf} = \frac{2u_*^2(h)}{u^2(h)}$$

where $u_*(h)$ (m·s^{-1}) is the friction velocity at canopy height with $u_*^2(h)$ being synonymous with the uniform profile of Reynolds stress at or above canopy height, i.e., the region $1 \leq \xi$ (or $h \leq z$), which is assumed to be the region of constant stress and (or) constant flux.

Critical to the success of the present model (as well as M97 and other similar analytical models) is the parameterization of the ratio $u_*(h)/u(h)$ as a function of $\zeta(h)$. This closes the set of equations by ensuring that $C_{surf} = C_{surf}(\zeta(h))$ is determined only from the model input (i.e., canopy structure characteristics). Here $u_*(h)/u(h)$ is adapted from M97 and Wang (2012) and is given as follows:

$$(10) \qquad \frac{u_*(h)}{u(h)} = c_1 - c_2 \exp[-c_3\zeta(h)]$$

where $c_1 = 0.38$, $c_3 = 15$, and $c_2 = c_1 + k/\log(\xi_{0G})$, and $k = 0.40$ is the von Karman constant. This particular value of c_1 has been adjusted from its original value of 0.32 in M97 to better fit the observed canopy wind and stress profiles. Further discussions and derivations of $u_*(h)/u(h)$ and C_{surf} can be found within the text and citations in M97.

To restate: The final (nondimensional) within-canopy wind profile is

$$(11) \qquad \frac{u(\xi)}{u(1)} = U_b(\xi)U_t(\xi) \quad \text{for } 0 \leq z \leq h$$

The nondimensional within-canopy profile of Reynolds stress is a modification of $U_t(\xi)$:
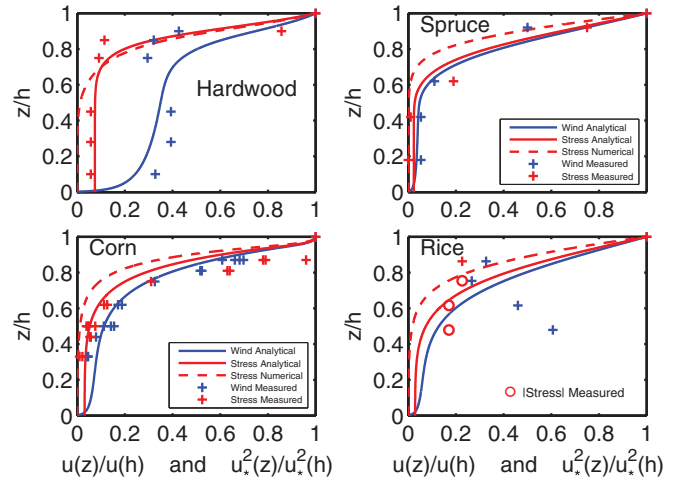
$$(12) \qquad \frac{u_*^2(\xi)}{u_*^2(1)} = \frac{\cosh[q_*N\zeta(\xi)/\zeta(h)]}{\cosh(q_*N)} \quad \text{for } 0 \leq z \leq h$$

where $q_* = q_a + q_b \exp(-q_cN)$, and $q_c = 0.60$, $q_b = 2/(1 - e^{-1})$, and $q_a = 4.02 - q_b$. These specific values for q_a, q_b, and q_c were estimated empirically as a compromise between satisfying two different and somewhat contradictory goals: namely, providing a good and more-or-less universal description of all the observed canopy profiles of Reynolds stress, $u_*^2(z)/u_*^2(h)$, while also providing reasonable estimates of d/h and z_0/h (next section). These divergent criteria are discussed in more detail in the following section, which is devoted to modeling results for d/h and z_0/h. Nonetheless, this study also tests the performance of another (and more standard) approach for estimating, $u_*^2(z)$: one that involves solving for the stress from the shear stress/drag equation

$$(13) \qquad \frac{du_*^2(\xi)}{d\xi} = c_d(\xi)ha(\xi)u^2(\xi)$$

the performance of which is also discussed in more detail in the next section.

Figures 3 and 4 are a series of plots comparing the modeled wind and stress profiles with their corresponding observed profiles (from Katul et al. (2004)) for the canopies shown in Figs. 1 and 2. Table 1 provides the details on the physical characteristics of these canopies. Also shown in Figs. 3 and 4 are the stress profiles corresponding to the numerical integration of eq. 13. It is worthwhile to note that regardless of the canopy type, eq. 13 usually underestimates the observed within-canopy stress profile within the lower portion of the canopy. Reducing this bias in the $u_*^2(\xi)$ profile was one of the two reasons for developing eq. 12 as an alternative to eq. 13. The second reason is discussed in the next subsection, which describes the model for z_0 and d.

Figures 3 and 4 indicate that the wind and stress models perform reasonably well and the wind profile is definitely more realistic than the uniform canopy wind profile of AB79. However, the comparison between the modeled wind speed and the observations for the hardwood canopy (upper left-hand side of Fig. 4) indicates that the present wind model (eq. 11) does not reproduce the often-observed secondary wind speed maximum within the

Table 1. Canopy parameters: from left to right, the first four columns are from Katul et al. (2004), whereas the last three columns are specific to the present study.

Canopy type	h (m)	PAI	C_d	d_1	$C_{d,equiv}$	$\zeta(h)$
Aspen	10	3.28	0.20	0		0.656
Scots pine	20	2.41	0.25	0		0.603
Jack pine	15	2.14	0.20	−0.7	0.27	0.578
Loblolly pine	24	3.78	0.20	0		0.756
Hardwood	22.5	4.93	0.15	+2	0.0925	0.456
Spruce	10	5.73	0.20	0		1.146
Corn	2.2	2.94	0.30	0		0.882
Rice	0.73	3.10	0.30	0		0.930

Note: h, height; PAI, plant area index; C_d, drag coefficient; $C_{d,equiv}$, $\zeta(h)$/PAI; $\zeta(h)$, drag area index.

lower half of the canopy (e.g., Shaw 1977). The present model's monotonicity may or may not be a weakness. In many cases, the observed secondary maximum is fairly weak or often nonexistent. In the case of prescribed burns or wildfires, it is completely unknown how a fire might affect the strength (or presence or absence) of the secondary maximum. Nonetheless, it is possible to construct a model wind profile that captures this secondary wind profile (e.g., Yi 2008; Queck and Bernhofer 2010; de Souza et al. 2016) but only at the cost of having to introduce two or more additional empirical fitting parameters. And once these parameters are fitted, the resulting wind profile may only apply to that specific data set to which it has been fitted. However, gaining the ability to simulate the secondary wind speed maximum does come with a cost, namely, increasing model complexity and the need to know a priori that the secondary wind speed maximum is a static feature of all possible canopy wind speed profiles and canopy species, foliage distribution, and foliage density. Unfortunately, there are no data that can give such assurance. The strengths of eq. 11 are its relative simplicity and the fact that it requires only a few easily estimated, physically based parameters.

On the other hand, describing the input parameter set for eq. 11 as easily measured is somewhat belied by the need to adjust d_1 such that $d_1 \neq 0$ for the jack pine and hardwood canopies (Table 1). Nonetheless, the general profile ($d_1 = 0$ and $p_1 = 0$ by default) can be re-established for these two canopies by reassigning C_d to $C_{d,equiv}$, where $C_{d,equiv}$ is defined as $\zeta(h)$/PAI and $\zeta(h)$ is computed with eq. 4 with $d_1 \neq 0$. Such adjustments to C_d do have physical interpretations. In the case of the hardwood canopy, $\zeta(h) \equiv C_{d,equiv}$PAI is about 40% less than $\zeta(h) \equiv C_d$PAI, suggesting that the individual canopy drag elements (mostly leaves in this case) may be aerodynamically sheltered by one another. Although aerodynamic sheltering tends to reduce the PAI exposed directly to the wind, for the present purposes, it is easier to subsume this effect directly into $C_{d,equiv}$. (Note that it is possible to produce the same quality fit to the hardwood data as shown in Fig. 4 by using the sheltering function, for which eq. 3 would have $p_1 \neq 0$ and $d_1 = 0$). The jack pine canopy is different. Here, $\zeta(h) \equiv C_{d,equiv}$PAI is about 40% greater than $\zeta(h) \equiv C_d$PAI, suggesting (Grant 1984) the possibility that the basic canopy aerodynamic drag elements are not individual needles but are larger clumped groupings of needles (shoots, twigs, branch-lets, etc.), which are likely to have significantly higher drag coefficients than an individual needle. This physical phenomenon is not the same as sheltering, but it may well be related. Nevertheless, again for the present purposes, these hardwood and jack pine "curve-fitting" exercises lead to the following conclusions: (*i*) the model is quite sensitive to the specific numerical value of the drag area index, $\zeta(h)$, and (*ii*) the present wind model is likely to have an inherent minimal uncertainty in C_d (or more precisely $\zeta(h)$) of about ±40%. Although this uncertainty is largely an unavoidable consequence of the present model's structure, it also tends to be unavoidable and nearly universal with all canopy flow models. Finally, it is also important to note that the

present wind profile model has only been evaluated against full canopies because those are the only canopy type for which there is an adequate amount of observational data. However, predicting fire spread with the RFSM in areas of partial or sparse canopy cover (e.g., savannas, semiarid shrublands, etc.) pose some complexities that may override such concerns.

First, even if the present wind model is found to provide an accurate description of within-canopy wind speed for areas of partial canopy cover, it is not clear that this is the correct measure of wind speed to be using. Rather, the wind speed in the open areas between trees or shrubs may be more important (it will certainly be higher). Second, areas of partial canopy cover can be patchy and often clumped. Such spatial inhomogeneities in the distribution of vegetation cover result in dispersive momentum fluxes (Finnigan 1985), which are correlated departures from a mean area average much the same way that Reynolds fluxes are correlated departures from temporal averages. These fluxes can display vertical structure within a canopy (Poggi et al. 2004; Moltchanov and Shavit 2013) and are generally small compared with Reynolds fluxes, except possibly within the lower half of a sparse canopy. Dispersive momentum fluxes are not considered at all by AB79 (because the concept of a dispersive flux had not yet been developed). Considering the present model estimates d and z_0 using the within canopy Reynolds stress profile (detailed in the next section), an attempt was made to assess their influence on WAF by augmenting the stress profile, $u_*^2(z)$, with a parameterization of the dispersive momentum flux (Poggi et al. 2004; Moltchanov and Shavit 2013). The results suggest that dispersive momentum fluxes do not influence the model calculations significantly; but again, given the lack of observational data on this subject and flow within sparse canopies in general, these results can only be considered preliminary.

### Stand roughness length and displacement height

Estimating the mid-flame wind speed, U^{MF} (m·s⁻¹), requires an input wind speed, U_H (ms⁻¹), measured at some reference height above the canopy, H (m), and usually assumes that the wind speed profile above the canopy is logarithmic:

$$(14) \quad U(z) = \frac{u_*}{k}\left[\ln\left(\frac{z-d}{z_0}\right) + \ln(\lambda_{rs})\right] = \frac{u_*}{k}\left[\ln\left(\frac{\lambda_{rs}(z-d)}{z_0}\right)\right]$$
$$\text{for } H \leq z \leq H + h$$

where $k = 0.4$ is the von Karman constant and $\ln(\lambda_{rs}) \geq 0$, where $1 \leq \lambda_{rs}$ (dimensionless) ≤ 1.25 (M87), is an influence function associated with the roughness sublayer (Raupach 1994, 1995), a region of enhanced turbulence just above and within the top of the canopy. In AB79, d and z_0 are fixed model parameters and the roughness sublayer is ignored ($\lambda_{rs} \equiv 1$). In the present study, d and z_0 are derived from the vegetation characteristics (M97) and $\lambda_{rs} = 1.25$ is assumed as a default value. This particular value of λ_{rs} was chosen over the original value of 1.07 (M87), because it produced more realistic values for z_0/h (see eq. 16 and Figs. 6 and 7). The sensitivity of WAF to the value of λ_{rs} is discussed in the following section.

Regardless of how d, z_0, and λ_{rs} are specified, they remain integral to this logarithmic profile, which itself is an approximation. Strictly speaking, eq. 14 is valid only for a neutrally stable atmosphere (i.e., no heat or moisture exchange between the surface, the vegetation, and the atmosphere). This is unlikely to be true during a fire, because the fire must create turbulent convective currents that heat the surrounding atmosphere, which, in turn, will cause the atmosphere to become convectively unstable. However, at present, quantifying this instability and its influence on the roughness sublayer during any given fire is not possible, so it is important to recognize that, just as with C_d and $C_{d,equiv}$, this approximation only increases the inevitable and unavoidable uncertainty to the model's predictions of WAF.

Fig. 5. The lines show the model's predicted non-dimensional canopy zero-plane displacement height, d/h, from eq. 15 as a function of canopy drag area index, $\zeta(h)$, for canopies with different heights of maximum foliage density, ξ_{max}. The symbols correspond to the model's predicted values of d/h for the smoothed plant surface distribution shape functions, $f_a(z/h)$ shown in Figs. 1 and 2, for each their corresponding values of $\zeta(h)$. In the case of the jack pine and hardwood canopies, $\zeta(h)$ is calculated using $C_{d,equiv}$ rather than C_d (see Table 1). [Colour online.]

Fig. 6. The lines show the model's predicted non-dimensional roughness length, z_0/h, from eqs. 16 and 15 as a function of canopy drag area index, $\zeta(h)$, for canopies with different heights of maximum foliage density, ξ_{max}. The symbols correspond to the model's predicted values of z_0/h for the smoothed plant surface distribution shape functions, $f_a(z/h)$ shown in Figs. 1 and 2, for each their corresponding values of $\zeta(h)$. In the case of the jack pine and hardwood canopies, $\zeta(h)$ is calculated using $C_{d,equiv}$ rather than C_d (see Table 1). [Colour online.]
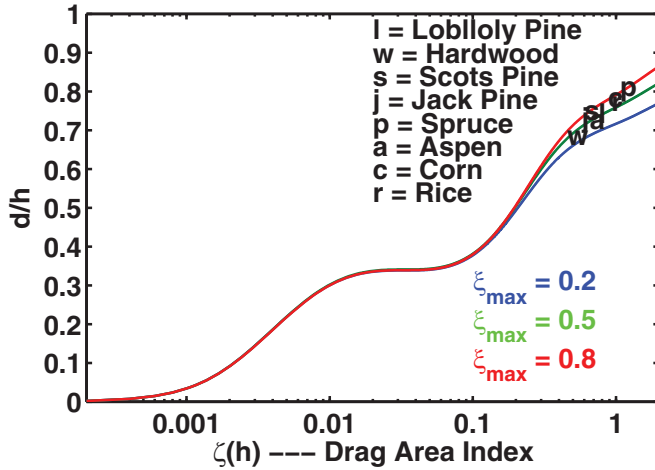
Following Thom (1971) and including the correction for the drag associated with the soil surface (Shaw and Pereira 1982), the canopy (or stand) zero-plane displacement height, d/h, is estimated as

(15) $$\frac{d}{h} = \left(1 - \frac{u_*^2(0)}{u_*^2(1)}\right)\frac{\int_0^1 \left[u_*^2(\xi)/u_*^2(1)\right]\xi d\xi}{\int_0^1 \left[u_*^2(\xi)/u_*^2(1)\right]d\xi}$$

and following M97, the surface (soil + vegetation) roughness length, z_0/h, is estimated as

(16) $$\frac{z_0}{h} = \lambda_{rs}\left(1 - \frac{d}{h}\right)e^{-\frac{k}{[u_*(h)/u(h)]}} = \lambda_{rs}\left(1 - \frac{d}{h}\right)e^{-k\sqrt{2/C_{surf}}}$$

Figures 5–7 show the model's predictions for d/h and z_0/h as functions of $\zeta(h)$ and canopy type. Figure 7 also includes comparisons between modeled and observed values of z_0/h and $1 - d/h$ for full canopies (boxed area). Not shown on any of these three figures are the results of assuming $\lambda_{rs} = 1.07$ or from using eq. 13, both of which produced values for z_0/h that were too low and (or) values of d/h that were too high, resulting in estimates of the normalized roughness lengths and displacement heights that were outside the observed values for a full canopy cover. The results from eq. 13 were much worse than those corresponding to $\lambda_{rs} = 1.07$. There are two things worthy of note concerning the results shown in these three figures. First, it is possible to improve on the model's ability to capture the full canopy cover indicated by the box of Fig. 7 simply by adjusting the values of q_a, q_b, and q_c of eq. 12. But to do so also degrades the quality of the fit that eq. 12 produces for the stress profiles shown in Figs. 3 and 4. Second, the present model is less sensitive to ξ_{max} than suggested in previous studies (Shaw and Pereira 1982; Massman 1987; Massman 1997).

Wind adjustment factors

AB79 define two different WAFs. The first case (WAF$_{sub}$) is for a subcanopy fire with flames of height h_{flame}, such that $z_{0G} < h_{flame} < h < h + H$.
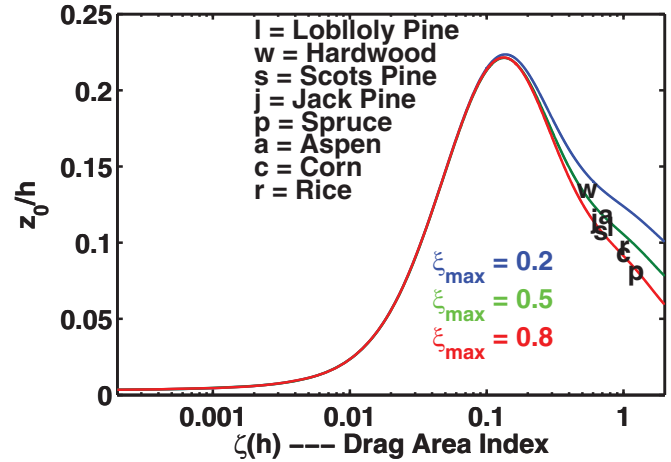
Fig. 7. This figure synthesizes the results in the previous two figures. The lines correspond to z_0/h vs. $1 - d/h$ from eqs. 16 and 15 for canopies with different heights of maximum foliage density, ξ_{max}. The symbols correspond to z_0/h vs. $1 - d/h$ for the smoothed plant surface distribution shape functions, $f_a(z/h)$ shown in Figs. 1 and 2. The boxed area encloses the observed range of values of z_0/h and $1 - d/h$ that correspond to full canopies, i.e., $0.10 \leq z_0/h \leq 0.13$ and $0.25 \leq (1 - d/h) \leq 0.33$. [Colour online.]
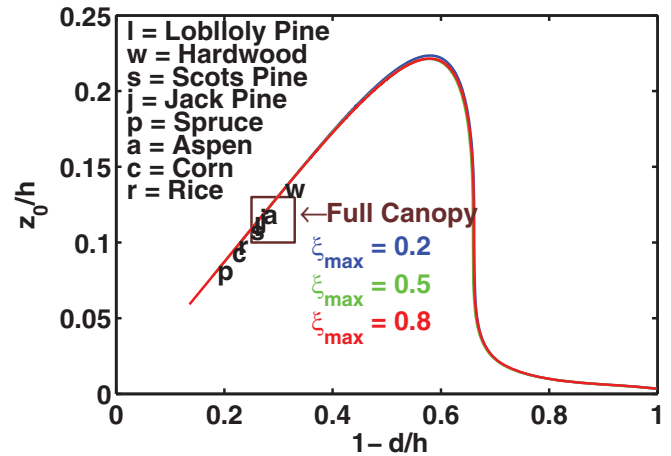
This case is intended to describe a fire with flame heights that are below the lowest branches of a forest canopy. The second case (WAF$_{above}$) is for a fire for which the canopy itself is burning and consequently for which the flames extend above the canopy, i.e., $z_{0G} < h < h_{flame} < h + H$, which describes a fire with a flame height that exceeds the canopy height but is still below the height of the wind measurement ($h + H$). An example of an above-canopy fire might be one that occurs in an open area without trees such as a grassland or shrubland. In this case, h corresponds to both the canopy height and the fuel bed height. Note that AB79 term the sub-canopy case an "under canopy" fire and the above-canopy case a "no-canopy" fire. AB79 arrive at this later "no-canopy" term,

because they lump any understory canopy with combustible ground material into the single category of ground fuel, thereby giving rise to the model constraint that the fuel bed height be the same as the canopy height for the "no-canopy" fire. Andrews (2012) termed a sub-canopy fire a "sheltered" fire, and she used the term "unsheltered" fire for the case of an above-canopy fire. But within this latter category, she also included a ground fire with no canopy present and a brush fire in which the canopy is burning, as well as any combustible ground material.

The general definition of the WAF is $U^{MF}/U(h + H)$, but the exact definition of the midflame wind speed, U^{MF}, depends on whether the fire is sub-canopy or above-canopy. For the sub-canopy case, U^{MF} is expressed analytically using eq. 11 in combination with eq. 14, yielding the following expression for WAF_{sub}:

$$(17) \quad WAF_{sub} = \frac{u(\xi_{mid})}{u(1)} \frac{U(h)}{U(h + H)}$$

$$= U_b(\xi_{mid})U_t(\xi_{mid}) \frac{\ln\left(\lambda_{rs}\left[\frac{1 - d/h}{z_0/h}\right]\right)}{\ln\left(\lambda_{rs}\left[\frac{H/h + 1 - d/h}{z_0/h}\right]\right)}$$

where $\xi_{mid} = \left(\frac{1}{2}h_{flame}\right)/h$ and by notational convention and functional continuity $U^{MF} \equiv u(\xi_{mid})$ and $U(h) \equiv u(1)$. The first term of this equation, $U_b(\xi_{mid})U_t(\xi_{mid})$, is the wind reduction factor between the canopy height and the height of the mid-flame, and the second or logarithmic term of the equation gives the reduction factor between the reference height $h + H$ and the canopy height h.

For the above-canopy case, U^{MF} is defined as the average wind speed over the height of the flame above the fuel bed, i.e., between h (the fuel height = shrub height or grass height, etc.) and $h + h_{flame}$. Combining this definition of U^{MF} with eq. 14 for the above-canopy wind speed profile yields the following definition for WAF_{above}:

$$(18) \quad WAF_{above} = \frac{\frac{1}{h_{flame}} \int_h^{h+h_{flame}} U(z)dz}{U(h + H)}$$

$$= \frac{\ln\left(\lambda_{rs}\left[\frac{h_{flame}/h + 1 - d/h}{z_0/h}\right]\right) - 1 + \delta \ln\left(\frac{1}{\delta} + 1\right)}{\ln\left(\lambda_{rs}\left[\frac{H/h + 1 - d/h}{z_0/h}\right]\right)}$$

where $\delta = \frac{1 - d/h}{h_{flame}/h}$.

Figure 8 shows WAF_{sub} and WAF_{above} as functions of drag area index, $\zeta(h)$, for three different sets of canopy parameters, listed in the figure caption. This figure demonstrates the importance of foliage density $\zeta(h)$ and canopy type (fuel/fire: sub-canopy vs. above-canopy) for estimating WAF. It is also worth noting the WAF appears to be rather insensitive to canopy structure or shape (ξ_{max} and σ_u and σ_l). The present model was also found to be nearly completely insensitive to whether $\lambda_{rs} = 1.25$ or 1.07. These last two insensitivities benefit the model because they reduce the amount of detailed information that is truly needed to make credible predictions. Nonetheless, the model's sensitivity to the ground surface roughness, z_{0G}, has yet to be assessed. This is done by comparing the results in Fig. 8 with those in Fig. 9.

Figure 9 demonstrates that the present model of WAF is, in fact, reasonably sensitive to z_{0G}. The selection of parameters for Figs. 8 and 9 differ only in the choice of z_{0G}/h; where for Fig. 8, $z_{0G}/h = 0.0025$ (model default), and for Fig. 9, $z_{0G}/h = 0.025$. That WAF_{sub} is far more sensitive to z_{0G} than is WAF_{above} should not be unex-

Fig. 8. WAF_{sub} and WAF_{above} vs. drag area index for the following set of model parameters: $z_{0G}/h = 0.0025$ and $\lambda_{rs} = 1.25$ (default values for all runs). For WAF_{sub}, $h = 10$ m, $h_{flame} = 2$ m, $H = 6.096$ m (20 ft), $\xi_{max} = 0.8$ ($\sigma_u = 0.1$, $\sigma_l = 0.6$), $\xi_{max} = 0.5$ ($\sigma_u = 0.4$, $\sigma_l = 0.5$), and $\xi_{max} = 0.2$ ($\sigma_u = 0.4$, $\sigma_l = 0.1$). For WAF_{above}, the same parameters are used, except that $h = 3$ m. Although $h_{flame} = 2$ m in both cases, the total flame height in the above-canopy case is now $h + h_{flame} = 5$ m, rather than 2 m (= h_{flame}) in the sub-canopy case. Note that the three curves that comprise WAF_{sub} and WAF_{above} are virtually identical to one another. [Colour online.]
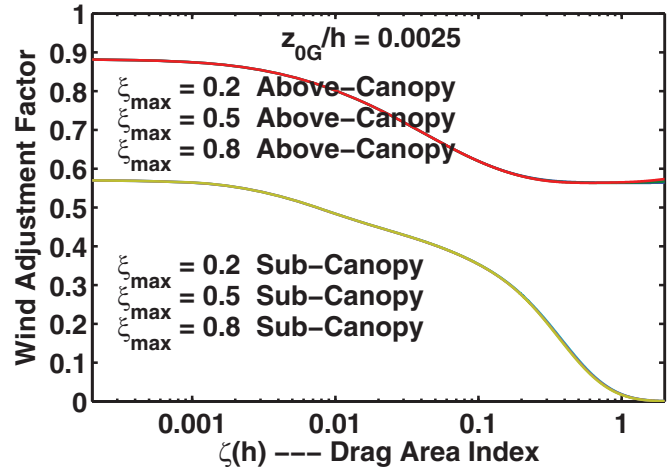

Fig. 9. WAF_{sub} and WAF_{above} as functions of the drag area index for exactly the same set of parameters as in Fig. 8, except that now $z_{0G}/h = 0.025$ (a 10-fold increase in the ground roughness length). Comparing this figure with Fig. 8 indicates that WAF_{sub} is relatively more sensitive to a change in the ground surface roughness length, z_{0G}, than WAF_{above}. As with Fig. 8, the three curves that comprise WAF_{sub} and WAF_{above} are virtually identical to one another. [Colour online.]
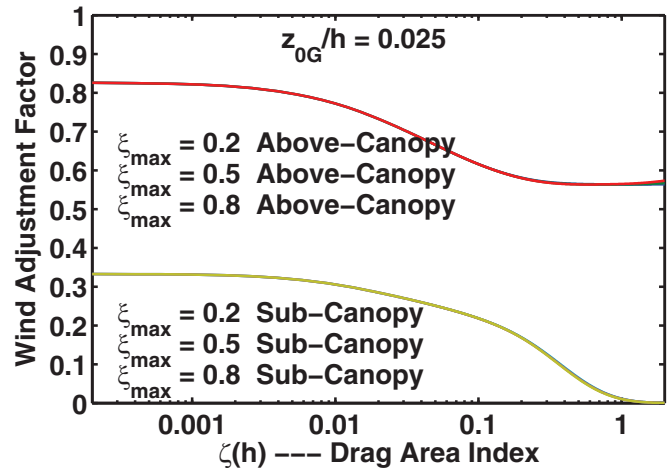
pected. In the case of a sub-canopy fire, the fire is likely to be contained within the lower half of the wind profile, which is dominated by the logarithmic profile and, therefore, dominated by z_{0G}.

Comparing these last two figures indicate that the model is sensitive to z_{0G} but that the sensitivity is greater for partial canopies or canopies that are less dense ($\zeta(h) \leq 0.20$–0.25) than for full canopy cover because the model results for either formulation of WAF shown in Figs. 8 and 9 become virtually indistinguishable as the canopy becomes increasingly denser (i.e., when $\zeta(h) \geq 0.50$). Consequently, depending on the nature of the canopy cover, this

sensitivity may or may not have practical implications for field applications. Nevertheless, the present conceptual basis for z_{0G} does create a potential ambiguity for how to define it for the sub-canopy fire case. This ambiguity is highlighted by comparing the present approach to modeling z_{0G} with the approach used in AB79. In the present (or new) model, z_{0G} is simply the ground surface roughness length, which is independent of the presence or absence of understory vegetation, and if there is an understory, the new model would include it as part of the plant surface distribution function. However, AB79 include the understory (along with any combustible material lying on the soil) as part of the fuel, and because they estimate z_{0G} solely on the basis of fuel roughness characteristics, their model incorporates the effects of the understory into z_{0G} rather than the plant surface distribution. Although it may not be possible to completely resolve this ambiguity with z_{0G}, the next section compares the modeling results from the original Rothermel–AB79 fire spread model with those produced with the new WAF–Rothermel fire spread model.

Performance with Rothermel's surface fire spread model

To facilitate the comparison between the AB79 model and the present model, it is necessary to relate PAI (used in the present model) with canopy cover, C (dimensionless; $0 \le C \le 1$), which is the corresponding variable in AB79. This relation is

$$(19) \qquad \text{PAI} = \frac{hF\beta\sigma}{2\pi}C$$

where F (dimensionless) is the canopy crown ratio (defined by AB79 and prescribed within the computer code of the BEHAVE program (Andrews 1986), which uses the Rothermel Fire Spread Equation) and $\beta\sigma = 10.6955$ m^{-1} (as derived and prescribed by AB79). Furthermore, each model also defines the drag coefficient somewhat differently. Therefore, to maintain fidelity with each model (and using notation from each model), the present model assigns $C_d = 0.2$ and the AB79 model assigns $\tilde{C}_D = 1$.

Figure 10 compares the Rothermel + AB79 results with two implementations of the Rothermel + NEW WAF model. The first implementation assigns $z_{0G} = 0.01$ m and the second implementation assigns z_{0G} following AB79 as $z_{0G} = 0.13D_{\text{fuel}} \approx 0.04$ m, where D_{fuel} is the fuel depth $\equiv$ height of the understory $= 1$ foot (0.305 m) for the sub-canopy case. For the above-canopy case, this figure includes only the results for $z_{0G} = 0.01$ m, because the 0.04 m model run is nearly identical to the present 0.01 m results (as found and discussed in the previous section). The new WAF model was also run for WAF$_{\text{sub}}$ and WAF$_{\text{above}}$ for both z_{0G} cases using both a constant and the asymmetric Gaussian plant surface distributions (eight model runs in all). Again, only the results for the uniform plant surface distribution are shown because the model WAF is almost totally insensitive to plant surface distribution (also discussed in the previous section).

Figure 11 shows the Rothermel fire spread rates as computed with the WAFs shown in previous figure. Not surprisingly these two figures are quite similar, so much so as to suggest that the Rothermel fire spread rates are basically linear functions of WAF.

There are two main conclusions to be drawn from the comparisons shown in these two figures. First, these two models of WAF differ significantly only for an above-canopy fire within sparse vegetation, i.e., a surface or area with canopy cover $C \le 0.20$–0.25 or so. Although it is not possible to say which model may be the better forecasting tool, this difference between these two models does suggest that the AB79 model produces slower rate of spread of above canopy fire at low values of canopy cover. Realistically, it is also difficult to say how meaningful this difference in modeled spread rates may be, because at this point, both models assume a continuous fuel bed to support fire spread, but for sparse cano-

Fig. 10. Comparison of WAF for the AB79 model and the present model. WAF$_{\text{sub}}$ and WAF$_{\text{above}}$ vs. canopy cover, C. The sub-canopy case, WAF$_{\text{sub}}$, assumes Fuel Model 2 (Anderson 1982; table 1), which is a forested overstory canopy and an understory of grass and forbs with a uniform plant surface distribution (i.e., $a(z) = \text{PAI}/h$), $z_{0G} = 0.01$ or 0.04 m [in brackets], $h = 10$ m, crown ratio = 0.5, $h_{\text{flame}} = D_{\text{fuel}}$ (where D_{fuel} is the fuel depth = height of the understory = 1 foot (0.305 m) for the sub-canopy case), and other parameters as discussed in the text. The above-canopy case, WAF$_{\text{above}}$, assumes Fuel Model 4 (Anderson 1982; table 1), which is a chaparral with a uniform plant surface distribution from canopy top to the ground surface, $z_{0G} = 0.025$ m, $h = 6$ feet (1.83 m), crown ratio = 1, and $h_{\text{flame}} = 2h$. [Colour online.]

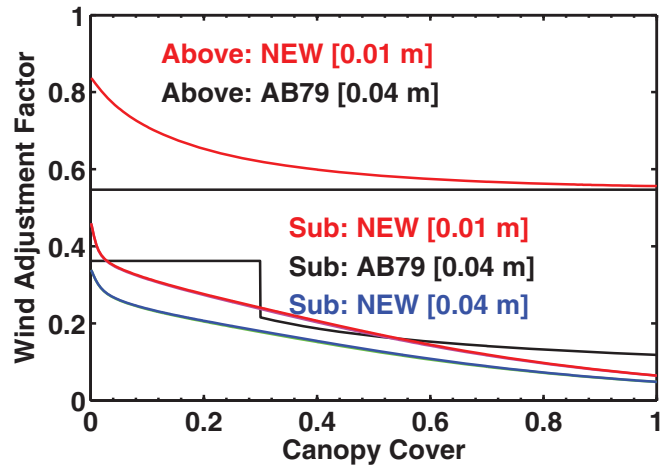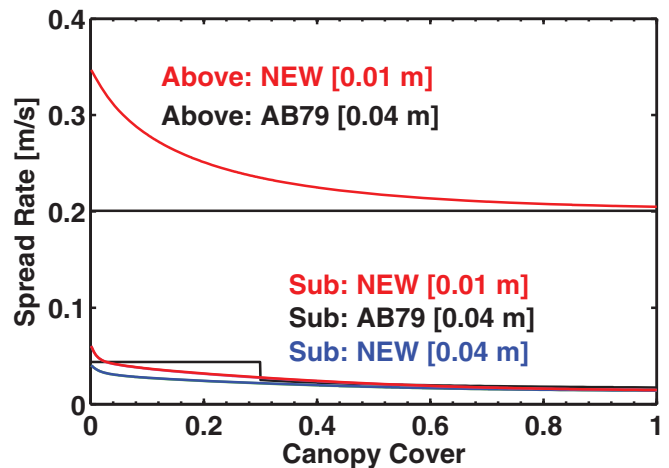**Fig. 11.** Fire spread rate (m·s^{-1}) from the RFSM with AB79 and the present model for the same set of parameters and fuel models as discussed in Fig. 10. [Colour online.]

pies, the vegetation and the associated fuel bed may be patchy and discontinuous. Second, the new model eliminates the discontinuity created by AB79 for sub-canopy fires (see $C = 0.3$, Figs. 10 and 11). Andrews (2012: fig. 20) discusses this discontinuity in more detail, but as she explains, the AB79 "Calculated WAF is based on surface bed depth if there is no or sparse overstory and on a description of the overstory if it exists at the site." Thus, AB79 does not provide for a smooth transition as between a sparse overstory and no overstory (i.e., as $C \to 0$). The switch between no overstory and a sparse overstory is algorithmically defined to occur when the crown fill (AB79, Andrews (2012)) is at 5%, which tends to occur within the range $0.2 \le C \le 0.4$.

Fig. 12. WAF from RFSM combined with the present model. The discontinuity at 10 m between the sub- and above-canopy cases is an artifact of the way WAF$_{sub}$ and WAF$_{above}$ are defined. The discontinuity in WAF results when a sub-canopy fire begins to consume the entire overstory, thereby transitioning to an above-canopy fire. [Colour online.]
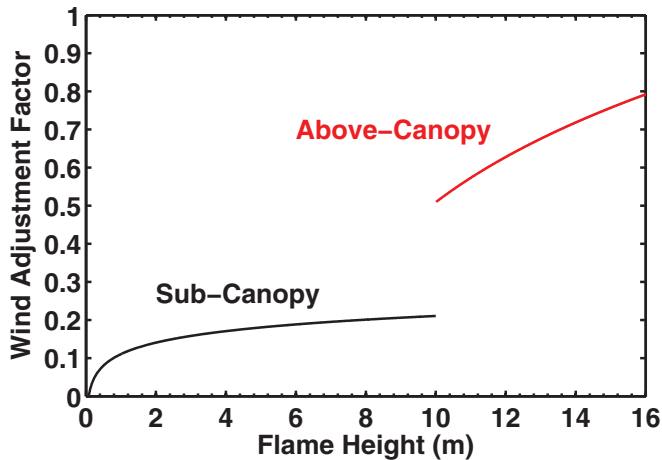
Finally, Fig. 12 shows that there is still a discontinuity in both the AB79 model and the new WAF model. The discontinuity at 10 m between the sub- and above-canopy cases is an artifact of the way WAF$_{sub}$ and WAF$_{above}$ are defined. In this (intentionally unrealistic) scenario, $h = 10$ m is fixed and only the flame height is varied. As long as the flames are beneath the canopy, the WAF$_{sub}$ is always defined relative to the mid-flame height, which here means that the mid-flame height above the ground is ≤5 m (or $h/2$ if $h \neq 10$ m). But when the fire extends above the canopy, then the effective mid-flame height is determined by integrating the logarithmic profile from h to $h + h_{flame}$, see eq. 18. In this case, the effective mid-flame height above the ground is now greater than 10 m. The discontinuity in WAF is introduced when a sub-canopy fire begins to consume the entire overstory and thereby begins to transition to an above-canopy fire.

Summary and recommendations

This study develops and tests a new, general canopy wind and Reynolds stress model that was designed for use with RFSM. The new model gave reasonable representations of observed within-canopy wind and Reynolds stresses for full canopies (PAI ≥ 1 or $\zeta(h) \geq 0.25$). However, due to the lack of data, it could not be tested for partial canopy covers (PAI < 1 or $\zeta(h) < 0.20$). Nonetheless, this new model does provide a smooth transition between full and partial canopies and it is more physically realistic than the original RFSM canopy wind model, developed by Albini and Baughman (1979) to predict the mid-flame wind speed from observations of above-canopy wind speeds. Unlike its predecessor, this new model allows for vertical structure in the canopy foliage area density and, consequently, for the canopy wind speed, as well as incorporating variations of canopy roughness length (z_0) and displacement height (d) as functions of canopy structure and foliage density. In general, this new model improves the performance of the RFSM, and we therefore recommend its use with the RFSM.

Beyond the RFSM, by improving upon Inoue's original 1963 exponential canopy wind profile model and some of its subsequent derivatives, this new model also offers the possibility of improving performance of other larger scale land surface and plant–atmosphere models. This might well be expected because the new model provides for better and more realistic descriptions of the canopy wind speed and canopy structure, and it satisfies the lower boundary condition ($u(z_{0G}) = 0$), which exponential-like wind speed profiles do not. Given the overall performance and physical realism of this new model, we are currently testing it with other large-scale land surface models.

References

Albini, F.A. 1981. A phenomenological model for wind speed and shear stress profiles in vegetation cover layers. J. Appl. Meteorol. **20**: 1325–1335. doi:10.1175/1520-0450(1981)020<1325:APMFWS>2.0.CO;2.

Albini, F.A., and Baughman, R.G. 1979. Estimating windspeeds for predicting wildland fire behavior. USDA For. Serv. Res. Pap. INT-221.

Anderson, H.E. 1982. Aids to determining fuel models for estimating fire behavior. USDA For. Serv. Gen. Tech. Rep. INT-122.

Andrews, P.L. 1986. BEHAVE: fire behavior prediction and fuel modeling system-BURN Subsystem, part 1. USDA For. Serv. Gen. Tech. Rep. INT-194.

Andrews, P.L. 2012. Modeling wind adjustment factor and midflame wind speed for Rothermel's surface fire spread model. USDA For. Serv. Gen. Tech. Rep. RMRS-GTR-266.

Cionco, R.M. 1965. A mathematical model for air flow in a vegetative canopy. J. Appl. Meteorol. **4**: 517–522. doi:10.1175/1520-0450(1965)004<0517:AMMFAF>2.0.CO;2.

Cowan, I.R. 1968. Mass, heat and momentum exchange between stands of plants and their atmospheric environment. Q. J. R. Meteorol. Soc. **94**: 523–544. doi:10.1002/qj.49709440208.

de Souza, C.M., Dias-Júnior, C.Q., Tóta, J., and de Abreu Sá, L.D. 2016. An empirical-analytical model of the vertical wind speed profile above and within an Amazon forest site. Meteorol. Appl. **23**: 158–164. doi:10.1002/met.1543.

Finnigan, J.J. 1985. Turbulent transport in flexible plant canopies. In The forest-atmosphere interaction. Proceedings of the Forest Environmental Measurements Conference, Oak Ridge, Tenn., 23–28 October 1983. Edited by B.A. Hutchison and B.B. Hicks. Springer, Dordrecht, Netherlands. pp. 443–480. doi:10.1007/978-94-009-5305-5_28.

Finnigan, J., Harman, I., Ross, A., and Belcher, S. 2015. First-order turbulence closure for modelling complex canopy flows. Q. J. R. Meteorol. Soc. **141**: 2907–2916. doi:10.1002/qj.2577.

Grant, R.H. 1983. The scaling of flow in vegetative structures. Boundary-Layer Meteorol. **27**: 171–184. doi:10.1007/BF00239613.

Grant, R.H. 1984. The mutual interference of spruce canopy structural elements. Agric. For. Meteorol. **32**: 145–156. doi:10.1016/0168-1923(84)90084-4.

Halldin, S. 1985. Leaf and bark area distribution in a pine forest. In The forest-atmosphere interaction. Proceedings of the Forest Environmental Measurements Conference, Oak Ridge, Tenn., 23–28 October 1983. Edited by B.A. Hutchison and B.B. Hicks. Springer, Dordrecht, Netherlands. pp. 39–58. doi:10.1007/978-94-009-5305-5_3.

Harman, I.N., and Finnigan, J.J. 2007. A simple unified theory for flow in the canopy and roughness sublayer. Boundary-Layer Meteorol. **123**: 339–363. doi:10.1007/s10546-006-9145-6.

Inoue, E. 1963. On the turbulent structure of airflow within crop canopies. J. Meteorol. Soc. Jpn. **41**: 317–326.

Katul, G.G., Mahrt, L., Poggi, D., and Sanz, C. 2004. One- and two-equation models for canopy turbulence. Boundary-Layer Meteorol. **113**: 81–109. doi:10.1023/B:BOUN.0000037333.48760.e5.

Massman, W.J. 1982. Foliage distribution in old-growth coniferous tree canopies. Can. J. For. Res. **12**: 10–17. doi:10.1139/x82-002.

Massman, W.J. 1987. A comparative study of some mathematical models of the mean wind structure and aerodynamic drag of plant canopies. Boundary-Layer Meteorol. **40**: 179–197.

Massman, W.J. 1997. An analytical one-dimensional model of momentum transfer by vegetation of arbitrary structure. Boundary-Layer Meteorol. **83**: 407–421. doi:10.1023/A:1000234813011.

Moltchanov, S., and Shavit, U. 2013. A phenomenological closure model of the normal dispersive stresses. Water Resour. Res. **49**: 8222–8233. doi:10.1002/2013WR014488.

Poggi, D., Katul, G.G., and Albertson, J.D. 2004. A note on the contribution of dispersive fluxes to momentum transfer within canopies. Boundary-Layer Meteorol. **111**: 615–621. doi:10.1023/B:BOUN.0000016563.76874.47.

Queck, R., and Bernhofer, C. 2010. Constructing wind profiles in forests from limited measurements of wind and vegetation structure. Agric. For. Meteorol. **150**: 724–735. doi:10.1016/j.agrformet.2010.01.012.

Raupach, M.R. 1994. Simplified expressions for vegetation roughness length and zero-plane displacement as functions of canopy height and area index. Boundary-Layer Meteorol. **71**: 211–216. doi:10.1007/BF00709229.

Raupach, M.R. 1995. Corrigenda. Boundary-Layer Meteorol. **76**: 303–304. doi:10.1007/BF00709356.

Raupach, M.R., Finnigan, J.J., and Brunei, Y. 1996. Coherent eddies and turbu-

lence in vegetation canopies: the mixing-layer analogy. Boundary-Layer Meteorol. **78**: 351–382. doi:10.1007/BF00120941.

Rothermel, R.C. 1972. A mathematical model for predicting fire spread in wildland fuels. USDA For. Serv. Res. Pap. INT-115.

Shaw, R.H. 1977. Secondary wind speed maxima inside plant canopies. J. Appl. Meteorol. **16**: 514–521. doi:10.1175/1520-0450(1977)016<0514:SWSMIP>2.0.CO;2.

Shaw, R.H., and Pereira, A.R. 1982. Aerodynamic roughness of a plant canopy: a numerical experiment. Agric. Meteorol. **26**: 51–65. doi:10.1016/0002-1571(82)90057-7.

Su, Z., Schmugge, T., Kustas, W.P., and Massman, W.J. 2001. An evaluation of two

models for estimation of the roughness height for heat transfer between the land surface and the atmosphere. J. Appl. Meteorol. **40**: 1933–1951. doi:10.1175/1520-0450(2001)040<1933:AEOTMF>2.0.CO;2.

Thom, A.S. 1971. Momentum absorption by vegetation. Q. J. R. Meteorol. Soc. **97**: 414–428. doi:10.1002/qj.49709741404.

Wang, W. 2012. An analytical model for mean wind profiles in sparse canopies. Boundary-Layer Meteorol. **142**: 383–399. doi:10.1007/s10546-011-9687-0.

Yi, C. 2008. Momentum transfer within canopies. J. Appl. Meteorol. Climatol. **47**: 262–275. doi:10.1175/2007JAMC1667.1.